Electrically Tunable Valley Dynamics in Twisted WSe_2/WSe_2 Bilayers

Giovanni Scuri,[1,*] Trond I. Andersen,[1,*] You Zhou,[1,2,*] Dominik S. Wild,[1] Jiho Sung,[1,2] Ryan J. Gelly,[1] Damien Bérubé,[3] Hoseok Heo,[1,2] Linbo Shao,[4] Andrew Y. Joe,[1] Andrés M. Mier Valdivia,[4] Takashi Taniguchi,[5] Kenji Watanabe,[5] Marko Lončar,[4] Philip Kim,[1,4] Mikhail D. Lukin,[1,†] and Hongkun Park[1,2,‡]

[1]*Department of Physics, Harvard University, Cambridge, Massachusetts 02138, USA*
[2]*Department of Chemistry and Chemical Biology, Harvard University, Cambridge, Massachusetts 02138, USA*
[3]*Department of Physics, California Institute of Technology, Pasadena, California 91125, USA*
[4]*John A. Paulson School of Engineering and Applied Sciences, Harvard University, Cambridge, Massachusetts 02138, USA*
[5]*National Institute for Materials Science, 1-1 Namiki, Tsukuba 305-0044, Japan*

(Received 14 December 2019; accepted 6 May 2020; published 28 May 2020)

The twist degree of freedom provides a powerful new tool for engineering the electrical and optical properties of van der Waals heterostructures. Here, we show that the twist angle can be used to control the spin-valley properties of transition metal dichalcogenide bilayers by changing the momentum alignment of the valleys in the two layers. Specifically, we observe that the interlayer excitons in twisted WSe_2/WSe_2 bilayers exhibit a high (>60%) degree of circular polarization (DOCP) and long valley lifetimes (>40 ns) at zero electric and magnetic fields. The valley lifetime can be tuned by more than 3 orders of magnitude via electrostatic doping, enabling switching of the DOCP from ~80% in the *n*-doped regime to <5% in the *p*-doped regime. These results open up new avenues for tunable chiral light-matter interactions, enabling novel device schemes that exploit the valley degree of freedom.

DOI: 10.1103/PhysRevLett.124.217403

Valleys represent the crystal momentum states where bands have an extremum [1–6]. Charge carriers or excitons in different valleys can exhibit markedly distinct properties [1], including different spin, optical selection rules, and Berry curvature, leading to a wealth of new physical phenomena such as the valley Hall [7,8] and Nernst effects [9,10]. Moreover, the valley degree of freedom can enable new ways of encoding and processing information beyond traditional schemes based purely on charge [11–13]. The realization of such applications relies on efficiently initializing a large valley polarization and achieving long valley and exciton lifetimes.

Transition metal dichalcogenides (TMDs) are a promising platform for valleytronics, as they host tightly bound excitons with coupled spin-valley properties that can be optically addressed via circularly polarized light [2,14–17]. A major obstacle to harnessing these properties in monolayer TMDs is the short lifetimes of intralayer excitons (0.1–1 ps) resulting from the sizeable electron-hole wave function overlap [18,19], as well as rapid valley mixing caused by exchange interactions [20–24]. Interlayer excitons in bilayer TMDs [13,25,26], consisting of an electron and a hole residing in two distinct TMD layers, present a promising route for overcoming these limitations. Because of the reduced wave function overlap, interlayer excitons can exhibit enhanced lifetimes that are 3–4 orders of magnitude longer than their intralayer counterparts [25,26] and tunable by an electric field [27].

Unfortunately, interlayer excitons in naturally occurring TMD bilayers exhibit rapid valley mixing, because valleys of opposite chirality are degenerate in energy and momentum [Fig. 1(a), top] [1,27–29]. Moreover, natural bilayers are inversion symmetric (the two layers are rotated 180° relative to each other); thus, as a whole, they do not exhibit net valley polarization [28,30] unless the symmetry is broken, e.g., with an electric field [31]. Consequently, most valleytronic studies involving interlayer excitons have focused on heterobilayers made of two different materials, such as WSe_2/MoS_2 [32] and $MoSe_2/WSe_2$ [12,13,33,34].

In this Letter, we show that the introduction of a twist angle between the layers can provide a new avenue for engineering the spin-valley properties of TMD bilayers, including homobilayers. Previously, the twist angle has been used to modify the resonance energy of excitons [35,36] and alter their properties due to moiré-induced spatial confinement and hybridization of bands [37–42]. Here, we tune the twist angle between the layers to control the momentum alignment of their respective valleys [Fig. 1(a), bottom], permitting long-lived interlayer exciton states with slow valley depolarization even at zero electric and magnetic fields. Importantly, we also demonstrate that the exciton and valley dynamics of twisted bilayers can be tuned via electrostatic doping.

To experimentally demonstrate twist-based spin-valley engineering, we fabricate optically addressable field-effect transistors that incorporate twisted WSe_2/WSe_2 bilayers (t-WSe_2/WSe_2) encapsulated in hexagonal boron nitride

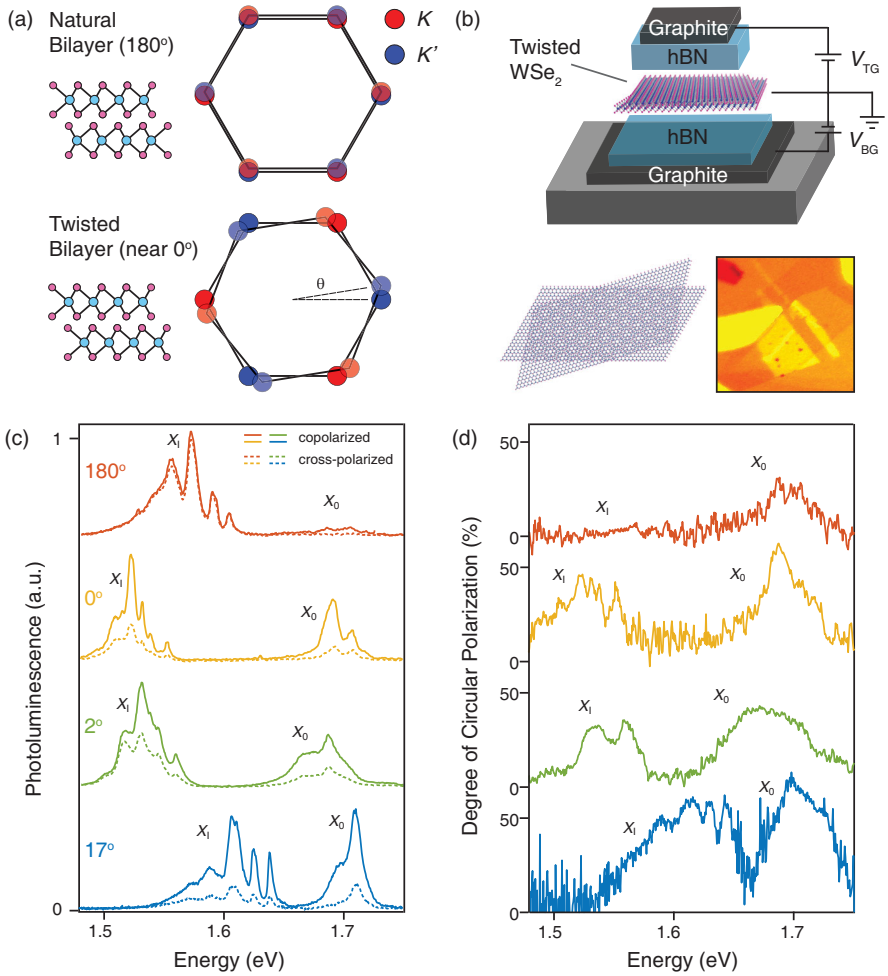

FIG. 1. Band engineering through twisting. (a) Side view and Brillouin zone alignment of natural (2H-stacked, top) and twisted homobilayers (bottom). The K and K' points are aligned in natural bilayers, but not in twisted structures. (b) Device schematic (top), illustration of a moiré pattern in a twisted WSe_2/WSe_2 bilayer (bottom left), and optical image of a device (bottom right). (c) Polarization-resolved PL spectra from bilayers with varying twist angles. All spectra are collected in the intrinsic regime. Solid (dashed) lines represent co- (cross-) polarized emission. X_0 and X_I indicate intralayer and interlayer exciton emission, respectively. (d) Degree of circular polarization calculated from the PL spectra in (c). While the natural bilayer (red) exhibits almost zero interlayer DOCP, the twisted devices show DOCP as high as 60%.

(hBN) [Fig. 1(b) and Supplemental Sec. I [43]]. The devices feature top and bottom graphene gates for independent control of doping and vertical electric field [27]. Using the tear-and-stack technique [44,45], we fabricate multiple such devices from high-quality exfoliated flakes, with target twist angles ranging from 0° to 17°. For comparison, we also make a device using a 2H-stacked natural bilayer (labeled as 180°).

Figure 1(c) shows polarization-resolved photoluminescence (PL) spectra from t-WSe_2/WSe_2 at different twist angles (see Supplemental Fig. S1 for additional twist angles [43]). These spectra are obtained with both of the graphene gates grounded, so that the TMD layers are intrinsic and under zero vertical electric field. At all twist angles, including the natural 2H bilayer, the spectra show two sets of peaks: The higher-energy peaks near 1.7 eV (X_0) are assigned to momentum direct (K-K) intralayer transitions [27,28,30], and the lower-energy peaks between 1.5 and 1.6 eV (X_I) are attributed to interlayer transitions [16,27,53,54]. This assignment is based on our measurements of the out-of-plane electric field dependence [Fig. 2(a), Supplemental Sec. II, and Supplemental Fig. S2 [43]], which show a zero (nonzero) linear Stark shift for intralayer (interlayer) excitons, consistent with previous studies [26,27]. Despite their weaker binding energies [26], the interlayer excitons have lower energies than the K-K intralayer excitons, indicating that they do not originate from the momentum direct K-K transition. Instead, the interlayer excitons arise from lower-energy transitions that are momentum indirect, as previously predicted for multilayer TMDs [16]. In particular, the interlayer exciton PL in natural bilayer WSe_2 was previously attributed to the K-Q transition [27].

As the twist angle is increased from 0° to 17°, the interlayer exciton peaks blueshift by almost 80 meV,

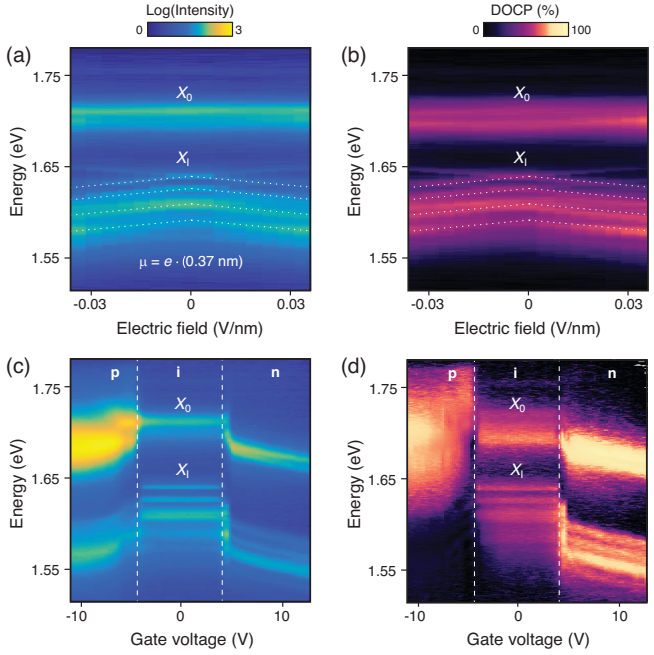

FIG. 2. Gate tunability of DOCP. (a) Out-of-plane electric field dependence of intra- and interlayer exciton PL from the 17°-twisted bilayer. While the intralayer excitons (X_0) do not shift with the electric field, the interlayer excitons (X_I) exhibit a Stark shift equivalent to an electron-hole separation of 0.37 nm. Opposite voltages are applied to the two gates (the hBN flakes have the same thickness) to apply an electric field while keeping the TMD intrinsic. (b) Electric field dependence of DOCP, showing that the DOCP is largely insensitive to the electric field. (c) Doping dependence of PL emission for intra- and interlayer excitons. The same voltages are applied to the two gates to dope the sample without applying an electric field. (d) Doping dependence of DOCP, showing switching from large (>80%) values in the *n*-doped regime to almost zero (<5%) in the *p*-doped regime.

consistent with reduced interlayer coupling [35,36,55–57] [Fig. 1(c)]. In all twisted structures, we observe four or five interlayer exciton peaks separated by 15–17 meV. We note that similar multipeak structures in twisted $MoSe_2/WSe_2$ heterostructures have been attributed to the confinement of interlayer excitons in moiré supercells [38]. In *t*-WSe_2/WSe_2 studied here, the multiple peaks are observed even in natural bilayers (as in Ref. [27]), and their spacing is independent of the twist angle, suggesting a different origin. Since their energy separation is similar to the optical phonon energy in WSe_2 [27,58], one possibility is that the peaks are phonon replicas [27]. Further experimental and theoretical studies are necessary to confirm this hypothesis, however.

The spin-valley properties of the interlayer excitons change drastically with the introduction of a twist angle between the two layers, as evidenced by the contrast between co- and cross-polarized emission signals (I_{co} and I_{cross}, respectively) in PL measurements. Upon illumination with circularly polarized light, the natural bilayer emits almost equal I_{co} and I_{cross}, whereas *t*-WSe_2/WSe_2 emits much stronger copolarized light [Fig. 1(c)]. Defining the degree of circular polarization (DOCP) as $(I_{co} - I_{cross})/(I_{co} + I_{cross})$, we find that, while the neutral interlayer exciton DOCP remains close to zero in natural bilayers, it reaches values as high as 60% in twisted bilayers [Fig. 1(d); see also Supplemental Fig. S3 and Supplemental Sec. III [43]]. Such high DOCP suggests much slower valley depolarization dynamics in *t*-WSe_2/WSe_2.

Next, we investigate the gate dependence of the interlayer excitons and their valley properties in the 17°-twisted bilayer device. Figures 2(a) and 2(b) show the electric field dependence of PL and the corresponding DOCP, obtained by applying equal and opposite voltages to the top and bottom graphene gates to eliminate effects of doping. From the Stark shift of the interlayer excitons, we extract an electron-hole separation of 0.37 nm, significantly smaller than the interlayer spacing, thus indicating that at least one of the carrier wave functions is partially delocalized between the layers. Importantly, both the extracted *e*-*h* separation and the DOCP are robust to the electric field, suggesting that the same interlayer exciton state dominates the PL signal at all fields explored here.

By instead applying equal voltages to the gates, we investigate the dependence on electrostatic doping in the absence of vertical electric field [Figs. 2(c)–2(d); see Supplemental Fig. S4 for similar behavior at a twist angle of 2° [43]]. In stark contrast to the electric field dependence, the DOCP is strongly dependent on doping. While the interlayer exciton DOCP exceeds 80% in the *n*-doped regime, it can be switched to almost zero (<5%) in the *p*-doped regime [Fig. 2(d)]. The DOCP stays relatively constant within each of the doping regimes and switches abruptly at their boundaries [Fig. 2(d)]. As in previous studies, the intralayer excitons do not exhibit this strong asymmetry [28].

Time-resolved PL measurements of the 17° twisted bilayer sample provide further insight into the exciton and valley dynamics [Figs. 3(a)–3(c), corresponding DOCP in Fig. 3(d)]. In the intrinsic regime, we fit the data with a biexponential decay [59] convoluted with the instrument response [dotted lines in Figs. 3(a) and 3(d)] and extract fast and slow timescales of $\tau_1 = 0.1$ ns and $\tau_2 = 0.9\,(1.0)$ ns for co- (cross-) polarized emission. Long interlayer exciton lifetimes are also observed for twist angles of 0° and 5°, which exhibit $\tau_2 = 2.0$ ns and $\tau_2 = 3.3$ ns, respectively (Supplemental Fig. S5 [43]). Similar to previous studies [24,60], we observe a 15 ps delay between the co- and cross-polarized emission, which causes a dip in the DOCP until both polarization branches reach the slow decay regime [Fig. 3(d)]. Fitting the DOCP in this regime with a linear coupled model (see Supplemental Sec. IV [43]), we extract a very long valley lifetime of 44 ns [dashed line in the inset in Fig. 3(d), lines corresponding to 5 and 10 ns

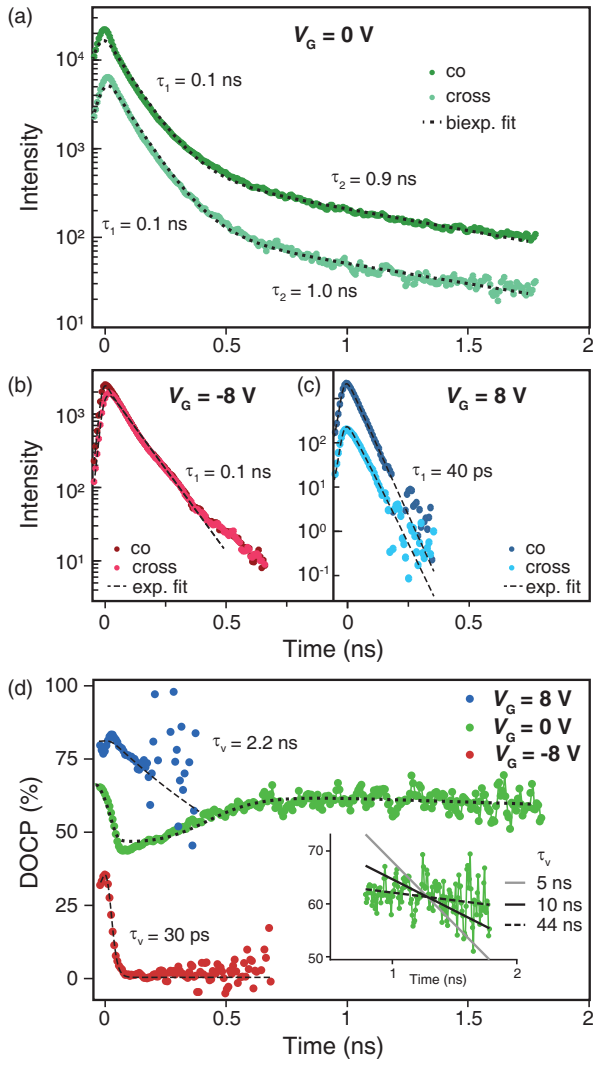

FIG. 3. Exciton and valley dynamics in twisted WSe_2. (a) Time-resolved measurements of co- and cross-polarized photoluminescence (dark and light green markers, respectively) from the 17°-twisted bilayer in the intrinsic regime. Black dotted lines are biexponential fits convolved with the instrument response (Supplemental Sec. IV [43]). The extracted slow and fast timescales are $\tau_1 = 0.1$ ns and $\tau_2 = 0.9\,(1.0)$ ns for co- (cross-) polarized emission. (b),(c) The same as in (a), but at $V_G = -8$ V and $V_G = 8$ V. Black dashed lines are fits based on the coupled linear model (Supplemental Sec. IV [43]). The extracted exciton and valley lifetimes are $\tau_1 = 0.1$ ns and $\tau_v = 30$ ps at $V_G = -8$ V and $\tau_1 = 40$ ps and $\tau_v = 2.2$ ns at $V_G = 8$ V. (d) Time-resolved DOCP corresponding to measurements in (a)–(c). Black dotted and dashed curves are calculated from fits in (a)–(c). Inset: Enlarged version of the long tail in the intrinsic regime, fitted with the linear coupled model (dashed line). The extracted valley lifetime is $\tau_v = 44$ ns. Lines corresponding to $\tau_v = 5$ ns (light gray) and $\tau_v = 10$ ns (dark gray) are shown for comparison.

shown for comparison], comparable to the best reported values in TMD heterobilayers [33].

In the doped cases, we focus on shorter timescales, because the exciton population and DOCP decay very rapidly in the n- and p-doped regimes, respectively. Fitting the data with the linear coupled model [43,60] [dashed lines in Figs. 3(b)–3(d)], we find that the initial exciton decay rate is faster in the n-doped regime ($\tau_1 = 40$ ps) than in the intrinsic and p-doped regimes ($\tau_1 = 0.1$ ns). Conversely, the valley lifetime is longer in the n-doped regime ($\tau_v = 2.2$ ns) than in the p-doped regime ($\tau_v = 30$ ps, similar to the instrument response time).

The observed polarization properties and their doping dependence can be understood from the band structure of t-WSe_2/WSe_2 bilayers. In natural (2H) bilayer WSe_2, recent angle-resolved photoemission spectroscopy measurements [61,62] and density functional theory calculations [27,63] suggest that the conduction band minimum (CBM) and valence band maximum (VBM) are located at the Q and K points, respectively. Our results suggest that these band extrema are conserved in t-WSe_2/WSe_2, consistent with recent studies in 3R-stacked bilayer WS_2 [64]. The extracted electron-hole separation of $d = 0.37$ nm [Fig. 2(a)] is smaller than the interlayer separation of $d_0 \sim 0.6$ nm [26] but larger than $d_0/2$, as expected for a K (hole) to Q (electron) transition, where the hole is localized in a single layer and the electron is partially delocalized between the layers (see Supplemental Sec. II for further discussion [43]). In particular, the extracted dipole moment is in excellent agreement with recent DFT calculations for 0° twisted bilayer WSe_2 [46], where the wave function at the Q point was predicted to have a 62%–38% distribution between the two layers (see Supplemental Sec. V [43] for further discussion).

A key difference in the band structures of natural and twisted WSe_2 bilayers is that the Q and K points are spin degenerate in the former but not in the latter [65]. Therefore, electrons and holes in natural bilayer WSe_2 do not need to acquire any energy or momentum to change spin, enabling rapid depolarization [Fig. 4(a)]. In contrast, valley depolarization of neutral interlayer excitons in twisted structures requires both carriers to scatter with phonons, acquire energy, and flip their spins [24,59] [Fig. 4(b)]. This is a much slower process, and the dynamics are instead likely governed by electron-hole exchange interactions [12,59,66]. However, since the interlayer excitons are indirect in both real and momentum space, even exchange interactions are expected to be slow [12,13,67]. In particular, they should be substantially slower than for momentum direct intralayer excitons, where such processes cause very short valley lifetimes (1–10 ps) in the intrinsic regime [24,68,69].

The observed hierarchy of valley lifetimes in the three doping regimes, i.e., $\tau_v(\text{intrinsic}) > \tau_v(n\text{-doped}) > \tau_v(p\text{-doped})$, is also well described by our band-structure considerations. In the p- and n-doped regimes, the depolarization dynamics of charged interlayer excitons are dominated by intervalley scattering [12,59,66], and, in contrast to the intrinsic regime, only one of the carriers needs to scatter, due to the additional resident charge in the

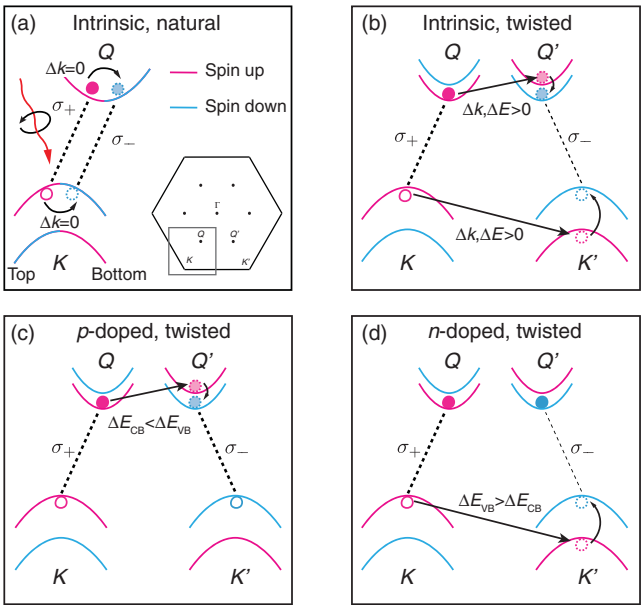

FIG. 4. Depolarization mechanisms in natural and twisted WSe_2/WSe_2 bilayers. (a) Depolarization in natural bilayer WSe_2 occurs simply through two spin-flip transitions (curved arrows), causing low DOCP. Magenta (cyan) bands indicate spin up (down) for electrons. The thickness of the dashed lines qualitatively represents the relative dominance of the σ_+ and σ_- recombination processes. Inset: Brillouin zone showing the location of the degenerate K and Q points of a natural bilayer as a whole. (b) Depolarization in twisted bilayer WSe_2 requires both a phonon-induced momentum kick (straight arrows) and a spin-flip transition (curved arrows) for both carriers, resulting in high DOCP and long τ_v. (c),(d) Since positively (negatively) charged excitons already have holes (electrons) at both the K and K' (Q and Q') points, only the electron (hole) must flip spin and shift in k space.

opposite valley. Positively charged excitons, which already have resident holes in both the K and K' valleys, require only scattering of the electron to depolarize [Fig. 4(c)]. Conversely, only the hole needs to scatter in negatively charged excitons [Fig. 4(d)]. These considerations indicate that the valley lifetime should be shorter in the doped regimes than in the intrinsic regime, as observed here. Our results in Fig. 3(d) suggest that the depolarization mechanism for holes is slower than for electrons in our twisted structures, consistent with the large spin-orbit coupling at the K point VBM and the resultant strong spin-valley locking for holes [28]. This is also in good agreement with a recent study on 3R-stacked bilayer WS_2 [64].

With regards to exciton lifetimes, we note that their doping dependence is influenced by various recombination processes, including both radiative and nonradiative ones. Further experimental and theoretical studies will be necessary to obtain a full understanding of the underlying microscopic phenomena that determine the doping dependence of exciton lifetimes.

The strong asymmetry in the degree of circular polarization shown in Fig. 2(d) is a result of the interplay between the depolarization and exciton decay dynamics, as implied from the expression $\mathrm{DOCP_{tot}} = \mathrm{DOCP_0}/(1 + 2\tau_1/\tau_v)$, where $\mathrm{DOCP_{tot}}$ and $\mathrm{DOCP_0}$ are the total (time-integrated) and initial DOCP, respectively. In the hole-doped regime, the depolarization timescale is shorter than τ_1 (30 ps and 0.1 ns, respectively), resulting in a low DOCP (<5%). In the electron-doped regime, on the other hand, τ_v is much longer than τ_1 (2.2 ns and 40 ps, respectively), so the observed DOCP is very large (>80%). Additionally, $\mathrm{DOCP_{tot}}$ is also affected by variations in $\mathrm{DOCP_0}$, which causes $\mathrm{DOCP_{tot}}$ to be higher in the n-doped regime than in the intrinsic regime, despite the fact that $\tau_1/\tau_v \ll 1$ in both regimes.

In conclusion, we have shown that the twist angle provides a new route for engineering the chiral optical properties of interlayer excitons in WSe_2/WSe_2 bilayers. Specifically, by changing the momentum separation of the valleys in the two layers, we achieve large valley polarization for long-lived interlayer excitons in t-WSe_2/WSe_2, in contrast to natural bilayers. Such valley polarization, which can be initialized and read out optically, is a direct consequence of the valley lifetime greatly exceeding the exciton lifetime. Moreover, in agreement with band structure considerations, the valley dynamics are highly tunable by electrostatic doping, enabling switching of the DOCP from more than 80% in the n-doped regime to <5% in the p-doped regime. Our results exemplify the power of twist-based engineering in van der Waals heterostructures and demonstrate that twisted TMD bilayers are a new promising platform for tunable chiral photonics and electrically switchable spin-valley-based devices. The coupling to functional structures, such as plasmonic metasurfaces [70–72], can further enhance chiral light-matter interactions and enable routing of electrically switchable chiral photons, thus opening up avenues for applications in quantum information storage and processing.

We acknowledge support from the Department of Defense Vannevar Bush Faculty Fellowship (N00014-16-1-2825 for H. P. and N00014-18-1-2877 for P. K.), NSF (PHY-1506284 for H. P. and M. D. L.), NSF CUA (PHY-1125846 for H. P. and M. D. L.), AFOSR MURI (FA9550-17-1-0002 for H. P., M. D. L. and P. K.), AFOSR DURIP (FA9550-09-1-0042 for M. L.), ARL (W911NF1520067 for H. P. and M. D. L.), the Gordon and Betty Moore Foundation (GBMF4543 for P. K.), ONR MURI (N00014-15-1-2761 for P. K.), and Samsung Electronics (for P. K. and H. P.). All fabrication was performed at the Center for Nanoscale Systems (CNS), a member of the National Nanotechnology Coordinated Infrastructure Network (NNCI), which is supported by the National Science Foundation under NSF Grant No. 1541959. K. W. and T. T. acknowledge support from the Elemental Strategy Initiative conducted by the MEXT, Japan, and the CREST (JPMJCR15F3), JST.

*These authors contributed equally to this work.
†To whom correspondence should be addressed. hongkun_park@harvard.edu,
‡To whom correspondence should be addressed. lukin@physics.harvard.edu

[1] D. Xiao, G.-B. Liu, W. Feng, X. Xu, and W. Yao, Coupled Spin and Valley Physics in Monolayers of MoS_2 and Other Group-VI Dichalcogenides, Phys. Rev. Lett. **108**, 196802 (2012).
[2] X. Xu, W. Yao, D. Xiao, and T. F. Heinz, Spin and pseudospins in layered transition metal dichalcogenides, Nat. Phys. **10**, 343 (2014).
[3] L. J. Sham, S. J. Allen, A. Kamgar, and D. C. Tsui, Valley-Valley Splitting in Inversion Layers on a High-Index Surface of Silicon, Phys. Rev. Lett. **40**, 472 (1978).
[4] A. Rycerz, J. Tworzydło, and C. W. J. Beenakker, Valley filter and valley valve in graphene, Nat. Phys. **3**, 172 (2007).
[5] Y. P. Shkolnikov, E. P. De Poortere, E. Tutuc, and M. Shayegan, Valley Splitting of AlAs Two-Dimensional Electrons in a Perpendicular Magnetic Field, Phys. Rev. Lett. **89**, 226805 (2002).
[6] O. Gunawan, Y. P. Shkolnikov, K. Vakili, T. Gokmen, E. P. De Poortere, and M. Shayegan, Valley Susceptibility of an Interacting Two-Dimensional Electron System, Phys. Rev. Lett. **97**, 186404 (2006).
[7] K. F. Mak, K. L. McGill, J. Park, and P. L. McEuen, The valley Hall effect in MoS_2 transistors, Science **344**, 1489 (2014).
[8] D. Xiao, W. Yao, and Q. Niu, Valley-Contrasting Physics in Graphene: Magnetic Moment and Topological Transport, Phys. Rev. Lett. **99**, 236809 (2007).
[9] M.-T. Dau *et al.*, The valley Nernst effect in WSe_2, Nat. Commun. **10**, 5796 (2019).
[10] X.-Q. Yu, Z.-G. Zhu, G. Su, and A. P. Jauho, Thermally Driven Pure Spin and Valley Currents via the Anomalous Nernst Effect in Monolayer Group-VI Dichalcogenides, Phys. Rev. Lett. **115**, 246601 (2015).
[11] W. Yao, D. Xiao, and Q. Niu, Valley-dependent optoelectronics from inversion symmetry breaking, Phys. Rev. B **77**, 235406 (2008).
[12] J. R. Schaibley, H. Yu, G. Clark, P. Rivera, J. S. Ross, K. L. Seyler, W. Yao, and X. Xu, Valleytronics in 2D materials, Nat. Rev. Mater. **1**, 16055 (2016).
[13] P. Rivera, H. Yu, K. L. Seyler, N. P. Wilson, W. Yao, and X. Xu, Interlayer valley excitons in heterobilayers of transition metal dichalcogenides, Nat. Nanotechnol. **13**, 1004 (2018).
[14] K. F. Mak, K. He, J. Shan, and T. F. Heinz, Control of valley polarization in monolayer MoS_2 by optical helicity, Nat. Nanotechnol. **7**, 494 (2012).
[15] H. Zeng, J. Dai, W. Yao, D. Xiao, and X. Cui, Valley polarization in MoS_2 monolayers by optical pumping, Nat. Nanotechnol. **7**, 490 (2012).
[16] K. F. Mak, C. Lee, J. Hone, J. Shan, and T. F. Heinz, Atomically Thin MoS_2: A New Direct-Gap Semiconductor, Phys. Rev. Lett. **105**, 136805 (2010).
[17] G. Scuri *et al.*, Large Excitonic Reflectivity of Monolayer $MoSe_2$ Encapsulated in Hexagonal Boron Nitride, Phys. Rev. Lett. **120**, 037402 (2018).
[18] C. Robert *et al.*, Exciton radiative lifetime in transition metal dichalcogenide monolayers, Phys. Rev. B **93**, 205423 (2016).
[19] G. Moody *et al.*, Intrinsic homogeneous linewidth and broadening mechanisms of excitons in monolayer transition metal dichalcogenides, Nat. Commun. **6**, 8315 (2015).
[20] M. M. Glazov, T. Amand, X. Marie, D. Lagarde, L. Bouet, and B. Urbaszek, Exciton fine structure and spin decoherence in monolayers of transition metal dichalcogenides, Phys. Rev. B **89**, 201302 (2014).
[21] T. Yu and M. W. Wu, Valley depolarization due to intervalley and intravalley electron-hole exchange interactions in monolayer MoS_2, Phys. Rev. B **89**, 205303 (2014).
[22] C. Mai, A. Barrette, Y. Yu, Y. G. Semenov, K. W. Kim, L. Cao, and K. Gundogdu, Many-body effects in valleytronics: Direct measurement of valley lifetimes in single-layer MoS_2, Nano Lett. **14**, 202 (2014).
[23] C. R. Zhu, K. Zhang, M. Glazov, B. Urbaszek, T. Amand, Z. W. Ji, B. L. Liu, and X. Marie, Exciton valley dynamics probed by Kerr rotation in WSe_2 monolayers, Phys. Rev. B **90**, 161302 (2014).
[24] A. Singh *et al.*, Long-Lived Valley Polarization of Intravalley Trions in Monolayer WSe_2, Phys. Rev. Lett. **117**, 257402 (2016).
[25] P. Rivera *et al.*, Observation of long-lived interlayer excitons in monolayer $MoSe_2 - WSe_2$ heterostructures, Nat. Commun. **6**, 6242 (2015).
[26] L. A. Jauregui *et al.*, Electrical control of interlayer exciton dynamics in atomically thin heterostructures, Science **366**, 870 (2019).
[27] Z. Wang, Y.-H. Chiu, K. Honz, K. F. Mak, and J. Shan, Electrical tuning of interlayer exciton gases in WSe_2 bilayers, Nano Lett. **18**, 137 (2018).
[28] A. M. Jones, H. Yu, J. S. Ross, P. Klement, N. J. Ghimire, J. Yan, D. G. Mandrus, W. Yao, and X. Xu, Spin–layer locking effects in optical orientation of exciton spin in bilayer WSe_2, Nat. Phys. **10**, 130 (2014).
[29] Z. Gong, G.-B. Liu, H. Yu, D. Xiao, X. Cui, X. Xu, and W. Yao, Magnetoelectric effects and valley-controlled spin quantum gates in transition metal dichalcogenide bilayers, Nat. Commun. **4**, 2053 (2013).
[30] G. Wang, X. Marie, L. Bouet, M. Vidal, A. Balocchi, T. Amand, D. Lagarde, and B. Urbaszek, Exciton dynamics in WSe_2 bilayers, Appl. Phys. Lett. **105**, 182105 (2014).
[31] S. Wu *et al.*, Electrical tuning of valley magnetic moment through symmetry control in bilayer MoS_2, Nat. Phys. **9**, 149 (2013).
[32] J. Kim *et al.*, Observation of ultralong valley lifetime in WSe_2/MoS_2; heterostructures, Sci. Adv. **3**, e1700518 (2017).
[33] P. Rivera, K. L. Seyler, H. Yu, J. R. Schaibley, J. Yan, D. G. Mandrus, W. Yao, and X. Xu, Valley-polarized exciton dynamics in a 2D semiconductor heterostructure, Science **351**, 688 (2016).
[34] A. Ciarrocchi, D. Unuchek, A. Avsar, K. Watanabe, T. Taniguchi, and A. Kis, Polarization switching and electrical control of interlayer excitons in two-dimensional van der Waals heterostructures, Nat. Photonics **13**, 131 (2019).

[35] A. M. van der Zande *et al.*, Tailoring the electronic structure in bilayer molybdenum disulfide via interlayer twist, Nano Lett. **14**, 3869 (2014).

[36] K. Liu, L. Zhang, T. Cao, C. Jin, D. Qiu, Q. Zhou, A. Zettl, P. Yang, S. G. Louie, and F. Wang, Evolution of interlayer coupling in twisted molybdenum disulfide bilayers, Nat. Commun. **5**, 4966 (2014).

[37] N. Zhang, A. Surrente, M. Baranowski, D. K. Maude, P. Gant, A. Castellanos-Gomez, and P. Plochocka, Moiré intralayer excitons in a $MoSe_2/MoS_2$ heterostructure, Nano Lett. **18**, 7651 (2018).

[38] K. Tran *et al.*, Evidence for moiré excitons in van der Waals heterostructures, Nature (London) **567**, 71 (2019).

[39] C. Jin *et al.*, Observation of Moiré excitons in WSe_2/WS_2 heterostructure superlattices, Nature (London) **567**, 76 (2019).

[40] E. M. Alexeev *et al.*, Resonantly hybridized excitons in moiré superlattices in van der Waals heterostructures, Nature (London) **567**, 81 (2019).

[41] K. L. Seyler, P. Rivera, H. Yu, N. P. Wilson, E. L. Ray, D. G. Mandrus, J. Yan, W. Yao, and X. Xu, Signatures of moiré-trapped valley excitons in $MoSe_2/WSe_2$ heterobilayers, Nature (London) **567**, 66 (2019).

[42] C. Jin *et al.*, Identification of spin, valley and moiré quasi-angular momentum of interlayer excitons, Nat. Phys. **15**, 1140 (2019).

[43] See Supplemental Material at http://link.aps.org/supplemental/10.1103/PhysRevLett.124.217403, for additional details regarding experimental methods, exciton characterization based on Stark shifts, and fitting models used for the time-dependent PL data. It includes Refs. [26,35,44–52].

[44] K. Kim *et al.*, van der Waals heterostructures with high accuracy rotational alignment, Nano Lett. **16**, 1989 (2016).

[45] Y. Cao, V. Fatemi, S. Fang, K. Watanabe, T. Taniguchi, E. Kaxiras, and P. Jarillo-Herrero, Unconventional superconductivity in magic-angle graphene superlattices, Nature (London) **556**, 43 (2018).

[46] V. Enaldiev, V. Zólyomi, C. Yelgel, S. Magorrian, and V. Fal'ko, Stacking domains and dislocation networks in marginally twisted bilayers of transition metal dichalcogenides, arXiv:1911.12804 [Phys. Rev. Lett. (to be published)].

[47] J. E. Padilha, H. Peelaers, A. Janotti, and C. G. Van de Walle, Nature and evolution of the band-edge states in MoS_2: From monolayer to bulk, Phys. Rev. B **90**, 205420 (2014).

[48] W. Li, T. Wang, X. Dai, X. Wang, C. Zhai, Y. Ma, and S. Chang, Bandgap engineering of different stacking WS_2 bilayer under an external electric field, Solid State Commun. **225**, 32 (2016).

[49] X. Fan, W. T. Zheng, J.-L. Kuo, D. J. Singh, C. Q. Sun, and W. Zhu, Modulation of electronic properties from stacking orders and spin-orbit coupling for 3R-type MoS_2, Sci. Rep. **6**, 24140 (2016).

[50] A. Weston *et al.*, Atomic reconstruction in twisted bilayers of transition metal dichalcogenides, arXiv:1911.12664.

[51] H. Yu, M. Chen, and W. Yao, Giant magnetic field from moiré induced Berry phase in homobilayer semiconductors, Natl. Sci. Rev. **7**, 12 (2020).

[52] F. Wu, T. Lovorn, E. Tutuc, I. Martin, and A. H. MacDonald, Topological Insulators in Twisted Transition Metal Dichalcogenide Homobilayers, Phys. Rev. Lett. **122**, 086402 (2019).

[53] A. Splendiani, L. Sun, Y. Zhang, T. Li, J. Kim, C.-Y. Chim, G. Galli, and F. Wang, Emerging photoluminescence in monolayer MoS_2, Nano Lett. **10**, 1271 (2010).

[54] J. Lindlau *et al.*, The role of momentum-dark excitons in the elementary optical response of bilayer WSe_2, Nat. Commun. **9**, 2586 (2018).

[55] P. K. Nayak *et al.*, Probing evolution of twist-angle-dependent interlayer excitons in $MoSe_2/WSe_2$ van der Waals heterostructures, ACS Nano **11**, 4041 (2017).

[56] J. Kunstmann *et al.*, Momentum-space indirect interlayer excitons in transition-metal dichalcogenide van der Waals heterostructures, Nat. Phys. **14**, 801 (2018).

[57] K. Wang *et al.*, Interlayer Coupling in Twisted WSe_2/WS_2 Bilayer heterostructures revealed by optical spectroscopy, ACS Nano **10**, 6612 (2016).

[58] Z. Jin, X. Li, J. T. Mullen, and K. W. Kim, Intrinsic transport properties of electrons and holes in monolayer transition-metal dichalcogenides, Phys. Rev. B **90**, 045422 (2014).

[59] G. Wang, A. Chernikov, M. M. Glazov, T. F. Heinz, X. Marie, T. Amand, and B. Urbaszek, Colloquium: Excitons in atomically thin transition metal dichalcogenides, Rev. Mod. Phys. **90**, 021001 (2018).

[60] R. Bertoni *et al.*, Generation and Evolution of Spin-, Valley-, and Layer-Polarized Excited Carriers in Inversion-Symmetric WSe_2, Phys. Rev. Lett. **117**, 277201 (2016).

[61] P. V. Nguyen *et al.*, Visualizing electrostatic gating effects in two-dimensional heterostructures, Nature (London) **572**, 220 (2019).

[62] E. J. Sie, T. Rohwer, C. Lee, and N. Gedik, Time-resolved XUV ARPES with tunable 24–33 eV laser pulses at 30 meV resolution, Nat. Commun. **10**, 3535 (2019).

[63] G.-B. Liu, D. Xiao, Y. Yao, X. Xu, and W. Yao, Electronic structures and theoretical modelling of two-dimensional group-VIB transition metal dichalcogenides, Chem. Soc. Rev. **44**, 2643 (2015).

[64] L. Du *et al.*, Robust circular polarization of indirect Q-K transitions in bilayer 3R WS_2, Phys. Rev. B **100**, 161404(R) (2019).

[65] A. Kormányos, V. Zólyomi, V. I. Fal'ko, and G. Burkard, Tunable Berry curvature and valley and spin Hall effect in bilayer MoS_2, Phys. Rev. B **98**, 035408 (2018).

[66] K. F. Mak, D. Xiao, and J. Shan, Light–valley interactions in 2D semiconductors, Nat. Photonics **12**, 451 (2018).

[67] F. Wu, T. Lovorn, and A. H. MacDonald, Theory of optical absorption by interlayer excitons in transition metal dichalcogenide heterobilayers, Phys. Rev. B **97**, 035306 (2018).

[68] K. Shinokita, X. Wang, Y. Miyauchi, K. Watanabe, T. Taniguchi, and K. Matsuda, Continuous control and enhancement of excitonic valley polarization in monolayer WSe_2 by electrostatic doping, Adv. Funct. Mater. **29**, 1900260 (2019).

[69] T. Yan, J. Ye, X. Qiao, P. Tan, and X. Zhang, Exciton valley dynamics in monolayer WSe_2 probed by the two-color

ultrafast Kerr rotation, Phys. Chem. Chem. Phys. **19**, 3176 (2017).

[70] A. A. High, R. C. Devlin, A. Dibos, M. Polking, D. S. Wild, J. Perczel, N. P. de Leon, M. D. Lukin, and H. Park, Visible-frequency hyperbolic metasurface, Nature (London) **522**, 192 (2015).

[71] L. Sun *et al.*, Separation of valley excitons in a MoS_2 monolayer using a subwavelength asymmetric groove array, Nat. Photonics **13**, 180 (2019).

[72] G. Hu *et al.*, Coherent steering of nonlinear chiral valley photons with a synthetic Au-WS_2 metasurface, Nat. Photonics **13**, 467 (2019).